# Evaluation of an optimal slip wall model for large-eddy simulation

**By M. P. Whitmore, S. T. Bose† AND P. Moin**

## 1. Motivation and objectives

The slip wall model for large-eddy simulation (LES) was first introduced by Bose & Moin (2014). In contrast to wall-stress models for LES, which typically rely on phenomenological arguments, the slip wall model is based on the slip boundary condition, which is derived mathematically from the application of a specific choice of low-pass filter to the Navier–Stokes equations. One benefit of this approach is that the slip wall boundary condition makes no assumption about the underlying state of the unresolved part of the boundary layer that it is modeling. Typical wall-stress models rely on a wall-stress boundary condition that embeds the assumption of a quasi-steady, thin, attached boundary layer. Because of this property, the slip wall model has higher potential for capturing complex flow phenomena such as turbulent flow separation, where common assumptions wall-stress modeling assumptions are invalid.

Despite the enhanced predictive potential of slip wall models for wall-modeled LES (WMLES), relatively little attention has been paid to understanding the proper scaling behaviors of slip lengths even in simple canonical flows. Much of the focus around the slip wall model since its conception has been on the development of models that dynamically adjust the slip length based on satisfaction of certain mathematical identities (e.g., invariance of the total Reynolds stress to test filtration), while invoking very few physical assumptions (Bose & Moin 2014; Bae et al. 2019). The results from these studies have shown sensitivity to closure of the slip length, and the proposed dynamic models are not robust across all tested flow configurations. In light of this, fundamental insight into the scaling behavior of an ideal slip wall model would be beneficial to help address present shortcomings. Yang et al. (2016) studied the slip boundary condition with the intention of providing a physical basis and, in the process, gave an expected scaling derived from comparison to the equilibrium wall-stress model. Similarly, Pradhan & Duraisamy (2022) investigated the slip length behavior through the use of an optimal Galerkin projection of channel direct numerical simulation (DNS) and other reference data onto a coarse-grained finite element basis. However, the form of the slip boundary condition used in these works differs from Bose & Moin (2014) in that a no-penetration condition is applied at the wall, and the wall stress is not primarily generated from a resolved Reynolds shear stress, as would be the case for a WMLES with a finite-width filter at the wall.

Recently, the slip wall model has been applied to a canonical case of smooth-body separation, where it has been shown to have potential for higher-fidelity predictions of turbulent smooth body separation (Whitmore et al. 2021, 2022). Despite this, the slip wall model based on a Prandtl mixing length used in these previous works, which performs adequately for regions with flow separation, gives poor predictions of skin friction in attached, approximately zero-pressure-gradient flows. This is especially true for flows

† Cadence Design Systems & ICME, Stanford University

that are at high Reynolds number and are coarsely resolved. These results have sparked a renewed interest in understanding the scaling behavior of the slip length in an ideal slip wall model, first for simple canonical flows, and also, eventually, for more complex non-equilibrium flows.

The purpose of this work is to develop a method to study the scaling behavior of an optimal slip wall model for WMLES. In order to do this, the model is framed as an optimization problem, for which some averaged skin friction data are supplied, and the slip lengths are solved in order to minimize the error with respect to the averaged skin friction data. Importantly, the focus of this method is on using *a posteriori* simulations for optimization, as this is the actual problem of interest when developing a wall model; therefore, the problem is framed such that all of the LES modeling choices are included as part of the system that needs to be optimized. In Section 2, the mathematical framework for this study is outlined, and the data sets used are listed. Section 3 gives results for the optimization method applied to a canonical case of turbulent channel flow. Section 4 focuses on the effect of the subgrid-scale model and proposes a novel model boundary condition for consistency between the subgrid-scale model and the slip wall model. Section 5 investigates some of the properties that arise in the limit of very high Reynolds numbers. Finally, some conclusions are offered in Section 6.

## 2. Mathematical framework

The LES equations are derived by applying a low-pass filter to the Navier–Stokes equations. The filtered velocity field is expressed as

$$\overline{u}_i(x',t) = \int_\Omega G(x',x)u_i(x,t)dx, \tag{2.1}$$

where $u_i$ is the velocity field, $G$ is the filter kernel, and $\overline{(\cdot)}$ represents the filtering operation. Assuming commutation between the filtering operation and differentiation, the LES equations for incompressible flow are written as

$$\frac{\partial \overline{u}_i}{\partial t} = -\frac{1}{\rho}\frac{\partial \overline{p}}{\partial x_i} - \frac{\partial}{\partial x_j}\left(\overline{u}_i\overline{u}_j\right) + \frac{\partial}{\partial x_j}\left(\nu\frac{\partial \overline{u}_i}{\partial x_j}\right) - \frac{\partial \tau_{ij}}{\partial x_j}\ ; \qquad \frac{\partial \overline{u}_i}{\partial x_i} = 0, \tag{2.2}$$

where $p$ is the pressure, $\rho$ is the density, and $\nu$ is the molecular viscosity. The subgrid-scale (SGS) stress tensor, $\tau_{ij}$, is defined as $\tau_{ij} \equiv \overline{u_iu_j} - \overline{u}_i\overline{u}_j$, which requires closure modeling. An eddy viscosity assumption is introduced to model the deviatoric part of the SGS term, such that $\tau_{ij} - (1/3)\tau_{kk}\delta_{ij} = -2\nu_t\overline{S}_{ij}$, where $\nu_t$ is the eddy viscosity and $\overline{S}_{ij}$ is the resolved strain rate tensor. The isotropic part of the SGS stress is included in the pressure. Except where noted, the eddy viscosity model used in this work is the dynamic Smagorinsky model (DSM) (Germano et al. 1991). These equations are now closed everywhere except the domain boundaries. In particular, wall boundary conditions for the LES equations must be chosen.

In the context of wall-stress modeled LES, the typical boundary conditions are

$$\nu\frac{\partial \overline{u}_s}{\partial n}\bigg|_w = \tau_w^m\ ; \qquad \overline{u}_n|_w = 0, \tag{2.3}$$

where $n$ is the wall-normal direction, $s$ is the local streamwise direction, and $(\cdot)|_w$ denotes evaluation at the wall. The quantity $\tau_w^m$ represents the stress prescribed by the wall model; for an equilibrium wall model, the stress is typically computed by matching the outer

LES solution to a prescribed inner solution of the velocity profile, or is alternatively found by assuming a Reynolds-averaged Navier–Stokes eddy viscosity profile and integrating a one-dimensional ordinary differential equation approximation of the thin boundary layer equations (Cabot & Moin 2000; Bose & Park 2018).

The slip boundary condition, assuming an isotropic slip length, has the form

$$\overline{u}_i|_w = C_{\text{slip}}\Delta_w \left.\frac{\partial \overline{u}_i}{\partial n}\right|_w ; \qquad i \in \{1,2,3\}. \tag{2.4}$$

The slip length, $C_{\text{slip}}\Delta_w$, for a finite-width filter is expected to be related to the computational grid size and, therefore, is expressed as the product of $\Delta_w$, the half-height of the first grid cell, and $C_{\text{slip}}$, a non-dimensional slip length coefficient. When the slip boundary condition is used, the wall shear stress vector, $\tau_{w,i}$, is expressed as

$$\langle \tau_{w,i} \rangle = \nu \left.\frac{\partial \langle \overline{u}_i \rangle}{\partial n}\right|_w - \langle \overline{u}_i \overline{u}_j \rangle|_w - \langle \tau_{ij} \rangle|_w \tag{2.5}$$

$$= \nu \left.\frac{\partial \langle \overline{u}_i \rangle}{\partial n}\right|_w - (C_{\text{slip}}\Delta_w)^2 \left. \left\langle \frac{\partial \overline{u}_i}{\partial n}\frac{\partial \overline{u}_j}{\partial n} \right\rangle \right|_w - \langle \tau_{ij} \rangle|_w , \tag{2.6}$$

where the first term on the right-hand side is the viscous stress, the second term is the resolved Reynolds stress, and the third term is the SGS stress tensor. The primary effect of the slip boundary condition is to impose a resolved Reynolds stress, with an approximately quadratic dependence on the slip length; however, the dependence cannot be fully parameterized by this quadratic relationship, as there are additional nonlinear effects through each term. Except where explicitly noted, the SGS stress is assumed to be zero at the wall for the calculations herein.

### 2.1. *Optimization method*

We now estimate the necessary slip length at the wall to reproduce a known wall stress stress distribution via an optimization procedure. We consider a boundary surface that has been discretized into a set of elements, and the skin friction distribution of the true solution, $C_f^{ref}$, is known. Then, an objective function is defined as

$$J\left(C_{\text{slip}}^{(k)}\right) = \frac{1}{2}\sum_k \left[\frac{1}{A_k}\int_{x\in\partial\Omega} w_k(x)\left\{C_f\left(x; C_{\text{slip}}^{(k)}\right) - C_f^{\text{ref}}(x)\right\} dx\right]^2 A_k, \tag{2.7}$$

where $k$ is the index of the boundary element that is used to discretize the slip lengths in space over the boundary surface. The local error values are computed as weighted area averages of the skin-friction error over the element, with $w_k$ being the test function and $A_k$ defined as the weighted area of the element. Note that this cost function is designed to allow for spatially varying slip lengths and skin friction values.

Given this cost function, we then seek slip length coefficients such that

$$C_{\text{slip}}^{(k),*} = \arg\min_{C_{\text{slip}}^{(k)}} J\left(C_{\text{slip}}^{(k)}\right). \tag{2.8}$$

Because this cost function is defined globally, and because it is not clear how to exactly parameterize changes in $C_f$ with respect to changes in the slip length coefficients, the cost function is treated as a black box for which function evaluations can be performed. In order to solve this minimization problem, an initial grid search is performed, and then the value found in the grid search is further refined by gradient descent that is done using

finite difference estimations of the cost function gradient. In order to do the evaluations of the cost function, it is also necessary to solve the flow for some amount of physical time; however, it is typically easy to define some outer flow scale over which to average—e.g., for a turbulent channel, this is done over some fixed number of eddy turnover times.

### 2.2. *Reference data*

The benefit of the proposed optimization method is that the required reference data are low dimensional. For example, a turbulent channel can be uniquely specified by a friction Reynolds number and a centerline velocity. Thus, the reference data can come from DNS statistics, experiments, or data fits.

The turbulent channel reference data are taken from DNS statistics at a range of friction Reynolds numbers: from $Re_\tau = 180$ to 10000 (Moser *et al.* 1999; del Álamo & Jiménez 2003; Hoyas & Jiménez 2006, 2008; Lozano-Durán & Jiménez 2014; Lee & Moser 2015; Hoyas *et al.* 2022; Oberlack *et al.* 2022). Additionally, the data fit proposed by Monkewitz (2017) is used to extrapolate to higher Reynolds numbers and is written as

$$U^+_{CL,ch} = \frac{1}{0.413} \ln \delta^+ + 5.88, \tag{2.9}$$

where $U_{CL,ch}$ is the channel centerline velocity and $\delta$ is the channel half-height. Note that $(\cdot)^+$ denotes nondimensionalization in inner units. While this formula is speculative in the limit of $Re_\tau \to \infty$, it is considered adequate for the purpose of the investigations below.

## 3. Turbulent channel results

The optimal slip length method is applied to turbulent channel flow for a Reynolds number range of $Re_\tau = 180$ to 10000. In addition to varying the Reynolds number, the simulations also vary the grid resolution, with isotropic resolution having nominal numbers of control volumes per channel half-height $N/\delta \in \{12, 20, 32, 40\}$. The purpose for varying both quantities is to observe whether there is any scaling behavior that is changing as a function of outer units, $y/\delta$, or inner units, $y^+$. The optimal slip length coefficients that resulted from the simulations are plotted in Figure 1 against the isotropic grid length scale, scaled in inner units.

The results of the optimal slip length coefficients appear to closely follow a smooth function behavior when plotted in inner units. Additionally, there appears to be minimal scaling behavior in outer units, as much of the data are nearly collapsed on this plot despite differences in resolution. The orderly collapse of the data is conducive to a parameterization with a smooth function. The parameterization introduced here is given by the form

$$C^m_{\text{slip}}(\Delta^+_w) = \left(0.19 - 0.02 \ln \frac{\Delta^+_w}{13}\right) \left\{1 - \exp\left[-\left(\frac{\Delta^+_w}{13}\right)^2\right]\right\}, \tag{3.1}$$

where $\Delta^+_w$ is the isotropic grid length scale scaled in inner units. The coefficients in this expression were fitted with the optimal slip length coefficient data via least squares. The first part of this functional form is similar to the scaling of the Reynolds stress from Townsend's attached eddy hypothesis (Marusic & Monty 2019). This suggests that while the derivation of the slip wall model is agnostic to the state of the local boundary layer, the ideal slip length may encode known physical scaling laws.

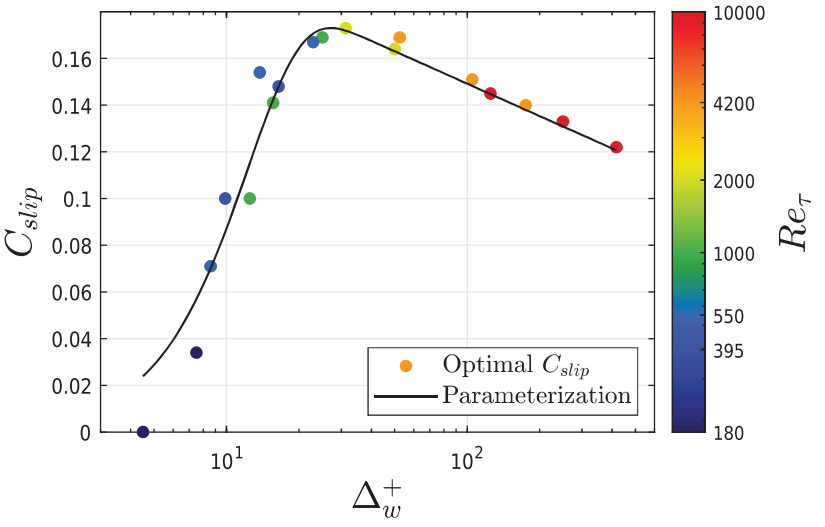


FIGURE 1. Optimal slip length coefficients computed for a turbulent channel flow at a range of Reynolds numbers and grid resolutions. A smooth function parameterization is plotted on top.

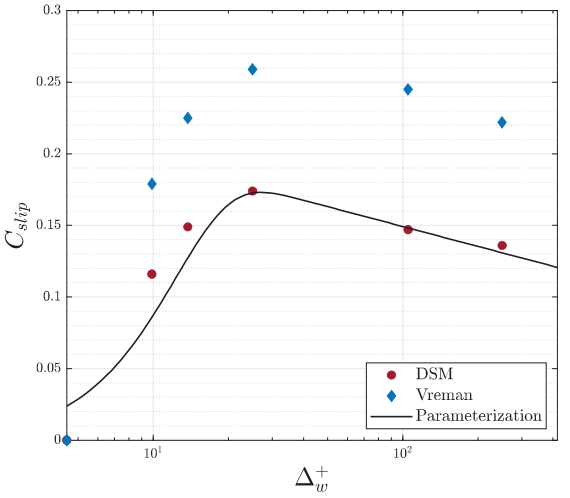


FIGURE 2. Results of the optimal slip length coefficients in the turbulent channel when using the dynamic Smagorinsky and Vreman subgrid-scale models.

## 4. Effect of subgrid-scale model

Up to this point, the simulations have been conducted using DSM. It is then natural to ask the question: how are the optimal slip length coefficients modulated by a change in the subgrid-scale model? To investigate this effect, we conduct an additional set of turbulent channel flow simulations using the Vreman subgrid-scale model (Vreman 2004). The comparison of the results when using the DSM and Vreman SGS models is shown in Figure 2. Unsurprisingly, when the SGS model is changed to the Vreman model, the optimal value of the slip coefficient increases across a range of Reynolds numbers. This

can be explained by the behavior of each SGS model near walls. Typically, the Vreman model tends to produce more dissipation to subgrid scales in the region near the wall than DSM does. As a result, because the LES has a reduced contribution from the resolved Reynolds stress, but the friction Reynolds number has not changed, the optimal slip length should increase to counteract this effect. This is seen in the figure, as the value of the ideal slip coefficient near its peak has increased from $\sim$0.17 to $\sim$0.26, which is a $\sim$50% increase in the peak value for this change of SGS models. An interesting property to note is that, despite this shift in the amplitude of the slip coefficient, the functional form that the optimal coefficients follow with respect to the grid length scale in inner units appears approximately the same. Nevertheless, the relatively large change in the size of the optimal slip coefficients indicates that methods to estimate slip lengths must be coupled to the interior SGS modeling.

In an effort to address this undesirable dependence of the optimal slip coefficient behavior on the SGS model, an SGS model boundary condition is introduced. In the previous results, the calculations were run assuming SGS stresses vanished at the wall (i.e., the eddy viscosity satisfied a homogeneous Dirichlet boundary condition), and all of the wall stress was produced from the slip velocities and viscous terms. This treatment could be viewed as inconsistent because, by including a resolved Reynolds stress term on the wall via the slip velocities, an SGS Reynolds stress term is implied to exist. Given this motivation to include an SGS stress contribution on the wall that is consistent with the slip boundary condition, we can then appeal to the derivation of the slip boundary condition to prescribe the behavior of the SGS stress.

### 4.1. *Subgrid-scale stress boundary condition*

The subgrid-scale stress tensor, $\tau_{ij}$, includes the grid-filtered quantity $\overline{u_i u_j}$; therefore, the definition of the differential filter of Germano (1986) can be applied to construct the form of the SGS stress tensor. Given the definition of the differential filter, the following expressions can be written

$$\overline{u_i u_j} - \frac{\partial}{\partial x_k}\left(\ell_p \frac{\partial}{\partial x_k}\overline{u_i u_j}\right) = u_i u_j, \tag{4.1}$$

$$\overline{u}_i - \frac{\partial}{\partial x_k}\left(\ell_p \frac{\partial}{\partial x_k}\overline{u}_i\right) = u_i, \tag{4.2}$$

where $\ell_p$ is a filter parameter. After multiplying Eq. (4.2) by itself for $\overline{u}_i$ and $\overline{u}_j$ and subtracting from Eq. (4.1), the unfiltered terms drop out, leaving a closed equation for $\tau_{ij}$. Assuming the singularity constraint on the filter parameter ($\ell_p \to 0$ at the wall) from Bose & Moin (2014), the SGS stress tensor for a differentially filtered field is found to satisfy the boundary condition

$$\tau_{ij}|_w - (C_{\text{slip}}\Delta_w)\left.\frac{\partial \tau_{ij}}{\partial n}\right|_w = \overline{u}_i\overline{u}_j|_w\,, \tag{4.3}$$

where $C_{\text{slip}}\Delta_w$ is the same slip length that is used for the velocity field, under the assumption that the same filter is applied to all velocity components. This boundary condition gives equations for the six components of the SGS stress tensor. Introducing an eddy viscosity model assumption for the form of the SGS stress tensor, the only free variable is the value of the eddy viscosity on the wall; thus, the system is overdetermined. By finding the least-squares solution of that system, a boundary condition is found for the

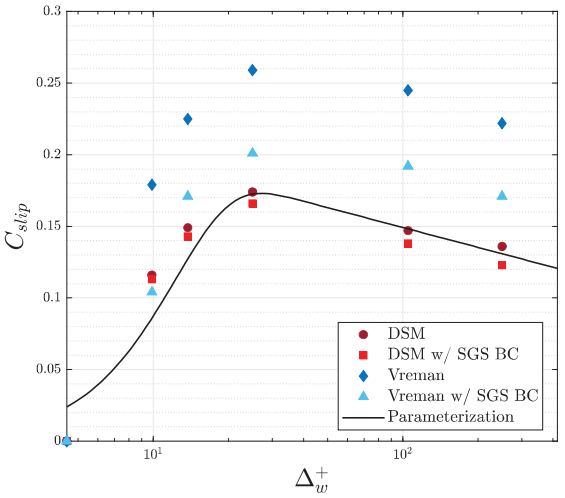


FIGURE 3. Results of the optimal slip length coefficients in the turbulent channel when using the dynamic Smagorinsky and Vreman subgrid-scale models, and with and without the inclusion of the derived subgrid-scale stress boundary condition.

eddy viscosity with the form

$$\nu_t|_w - C_{\nu_t}\Delta_w \left.\frac{\partial \nu_t}{\partial n}\right|_w = f_{\nu_t}|_w\,, \tag{4.4}$$

where $C_{\nu_t}$ represents a modified slip length coefficient for the eddy viscosity, and $f_{\nu_t}$ is a right-hand-side term. These quantities are defined in terms of the tensor contractions

$$C_{\nu_t} = C_{\text{slip}}\frac{\beta_{ij}\overline{S}_{ij}}{\beta_{kl}\beta_{kl}}; \qquad f_{\nu_t} = \frac{-\overline{u}_i\overline{u}_j\beta_{ij}}{2\beta_{kl}\beta_{kl}}, \tag{4.5}$$

where $\beta_{ij} \equiv \overline{S}_{ij} - C_{\text{slip}}\Delta_w\left(\partial\overline{S}_{ij}/\partial n\right)$, with all quantities evaluated at the wall. The result is an inhomogeneous Robin boundary condition for the eddy viscosity that is defined in terms of contractions of grid-filtered quantities and the velocity slip length.

The eddy viscosity boundary condition in Eq. (4.4) is employed in the turbulent channel, and the results of the optimal slip length coefficients are shown in Figure 3. The results show that with the SGS boundary condition, the optimal coefficient values when using the Vreman model decrease over the entire range of Reynolds numbers studied. Notably, the peak of the slip coefficients with the Vreman model, which showed a ∼50% discrepancy with the peak for DSM, shows only a ∼20% discrepancy with DSM at the peak values when the SGS boundary condition is included. It is also interesting to note that when the SGS boundary condition is applied, optimal slip length coefficients for DSM change only slightly. It can be interpreted from the results that by imposing a coupling between the velocity slip boundary condition and the SGS model, the WMLES is able to settle into a more consistent solution despite the change in SGS model. Additionally, the agreement of the results when using DSM with and without the SGS boundary condition implies some level of consistency between the dynamic model and the low-pass filter that is implied through the slip boundary condition for the velocity. The improved agreement of the results when this boundary condition is applied is promising because it

suggests that under the appropriate assumptions with the proper coupling, it is possible for LES results to achieve relative consistency even when model choices are varied.

## 5. Investigation of the $Re_\tau \to \infty$ limit

For WMLES, it is interesting to ask the question of what the wall model behavior is in the limit of the friction Reynolds number approaching infinity. Physically, this limit would be characterized by a viscous length scale becoming vanishingly small with respect to the boundary layer thickness, $1/Re_\tau = \delta_\nu/\delta \to 0$. Assuming the flow is attached everywhere, the wall would act as an infinitesimally thin vortex sheet (Pullin *et al.* 2013), while the outer flow would strongly resemble an inviscid flow. However, for any flow that exhibits flow separation, even the outer flow is significantly perturbed from its inviscid limit due to the finite displacement arising from the separation bubble itself. Traditional wall-stress models for WMLES rely in some form on the law of the wall to fit a solution and find a wall stress. This method, when taken to the limit of $Re_\tau \to \infty$, would produce a boundary condition that is essentially an inviscid or stress-free boundary condition. Therefore, a typical wall-stress model would become inconsistent when applied to this limiting case.

The slip wall model is worth investigating in this limit because it would not necessarily suffer from the same issue as a wall-stress model. In principle, the mathematical arguments that lead to the slip boundary condition would still be valid in this limit. Therefore, we proceed with the previous method to investigate the asymptotic behavior of the optimal slip length by simulating channels with asymptotically large Reynolds numbers. In order to perform these simulations, we need to have an estimate for the channel centerline velocity, $U^+_{CL}$, for Reynolds numbers far beyond those simulated in channel DNS. To do this, we use the data fit proposed by Monkewitz (2017), which is written in Eq. (2.9). A number of channels are simulated for the range $\log_{10} Re_\tau \in [5, 10]$, which goes beyond the available DNS data by six orders of magnitude in Reynolds number. The results of these simulations are shown in Figure 4.

Figure 4 shows that at the highest Reynolds numbers, the optimal slip coefficient continues to decay, but does so increasingly slowly. The results appear such that the optimal slip coefficient may asymptote to a finite value in the limit. This differs from the behavior of a wall-stress model, which becomes a stress-free boundary condition in the same limit. The case under which a slip wall boundary condition would collapse to a stress-free boundary condition would be the case where the slip length becomes infinitely large as the Reynolds number is increased, i.e., $u_w = C_{\text{slip}}\Delta(\partial u/\partial n)_w$ becomes $(\partial u/\partial n)_w \approx 0$. It is clear from the plot that this case is not approached. Additionally, while it is difficult to say from the current data what the value of the asymptote might be, it seems unlikely that the optimal slip coefficient is approaching zero; this would be a statement that the no-slip boundary condition is the ideal boundary condition in the $Re_\tau \to \infty$ limit. Therefore, it appears most plausible that the slip coefficient is approaching a finite value in the limit.

Next, the behavior of this slip length with respect to the dynamic Smagorinsky coefficient of the simulations is explored. Figure 5 shows the comparison of the optimal slip coefficients to the dynamically computed Smagorinsky coefficient in the first grid cell from the wall. From this result, it appears clear that the Smagorinsky constant, $C_s$, computed from DSM is plateauing in the limit of high Reynolds number. Additionally, the slip length coefficient and Smagorinsky constant are similar in magnitude. Due to their

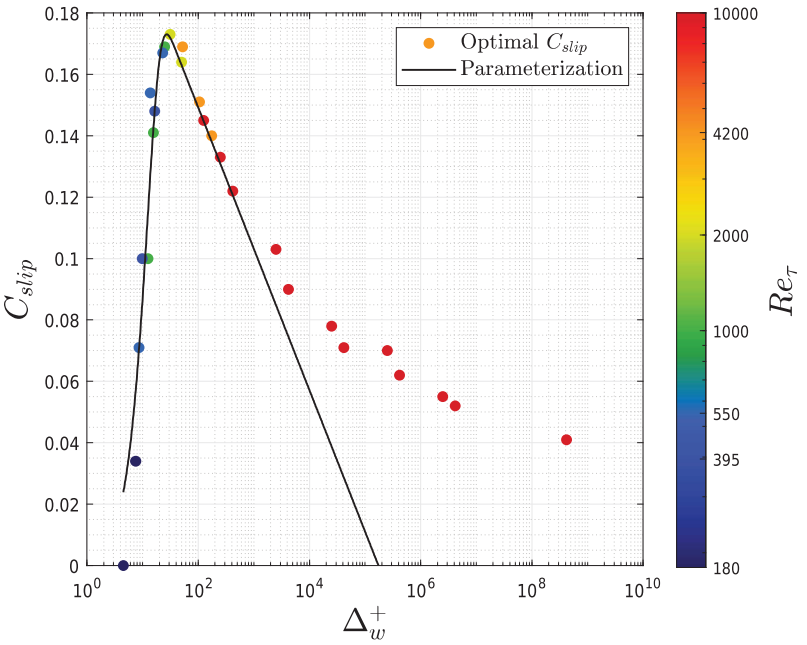


FIGURE 4. Results of the optimal slip length for turbulent channel flows including the very large Reynolds number cases extracted from the fit in Eq. (2.9). Note that the color scale is capped at the highest DNS Reynolds number and the extrapolated Reynolds number results are saturated.

similar orders of magnitude, and potentially similar plateau behavior at high Reynolds number, we can then try to relate these coefficients in the limit $Re_\tau \to \infty$.

First, we assume an equivalence of total shear stress at the height of the first grid cell and the wall

$$-\langle u'v'\rangle|_1 + \nu \left.\frac{\partial\langle u\rangle}{\partial n}\right|_1 + \alpha y_1 \frac{\partial\langle p\rangle}{\partial s} + \langle \tau_{sn}\rangle|_1 = -\langle u'v'\rangle|_w + \nu \left.\frac{\partial\langle u\rangle}{\partial n}\right|_w , \tag{5.1}$$

where $\alpha \sim O(1)$ assuming $\partial\langle p\rangle/\partial n$ is small in the boundary layer and assuming that the SGS stress vanishes at the wall. Then, if we further assume the discrete velocity gradient to be the same at the first cell and the wall and the streamwise pressure gradient to be small, then we are left with

$$-\langle u'v'\rangle|_1 + \langle \tau_{sn}\rangle|_1 \approx -\langle u'v'\rangle|_w . \tag{5.2}$$

Next, assuming in the limit of $Re_\tau \to \infty$ that the resolved Reynolds shear stress is much smaller than the SGS component, $-\langle u'v'\rangle \ll \langle \tau_{sn}\rangle$, we can approximately balance the terms

$$\langle \tau_{sn}\rangle|_1 \approx -\langle u'v'\rangle|_w . \tag{5.3}$$

Let $-\langle u'v'\rangle|_w \approx c_{uv}\langle u'^2\rangle\langle v'^2\rangle|_w$, where $c_{uv}$ is a correlation coefficient that is assumed to be constant in the high $Re_\tau$ limit. Further, assume that $\langle v'^2\rangle|_w \approx A\,\langle u'^2\rangle|_w$, where $A$ is a constant describing the anisotropy. This leads to

$$\langle \tau_{sn}\rangle|_1 \approx K_1\,\langle u'^2\rangle|_w , \tag{5.4}$$

where $K_1$ is some unspecified coefficient. If we then scale the velocity fluctuation on the

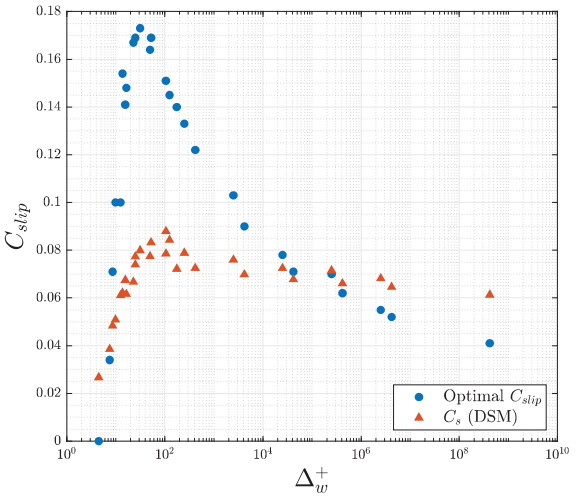


FIGURE 5. Optimal slip length coefficients from turbulent channel flow plotted alongside the dynamic Smagorinsky coefficient in the first grid cell.

wall with the definition of the slip length, and scale the subgrid stress with its definition,

$$\langle u'^2 \rangle\big|_w \approx K_2 \left(C_{\text{slip}} \Delta_w\right)^2 \left\langle \frac{\partial u'}{\partial n}^2 \right\rangle; \qquad \langle \tau_{sn} \rangle\big|_1 \approx \left(C_s \Delta\right)^2 \left\langle \frac{\partial u'}{\partial n}^2 \right\rangle, \tag{5.5}$$

where $K_2$ is another unspecified coefficient, we arrive at, in the limit of $Re_\tau \to \infty$,

$$\Rightarrow C_{\text{slip}} \sim K_3 C_s, \tag{5.6}$$

where $K_3$ is some coefficient, which is conjecturally less than unity. This analysis suggests that, if the Smagorinsky constant is plateauing in this limit, then the slip length coefficient should plateau at some constant factor times that value. Figure 5 does not contradict this conjecture; however, the present data are not sufficient to demonstrate such a plateau of the slip length coefficient in this limit.

## 6. Conclusions

An optimization framework is introduced in order to understand the scaling behavior of an ideal slip wall model for LES. This optimization framework is applied to a turbulent channel flow for a wide range of Reynolds numbers covered by reference data. The ideal slip length coefficients in the channel result in a smooth function profile that is conducive to parameterization by the grid length scale in inner units and is similar to the scaling of turbulent fluctuations from the attached eddy hypothesis. The effect of changing the SGS model is studied, and an SGS boundary condition is developed and used to address some of the discrepancy when changing SGS model. Lastly, the behavior of the optimal slip length coefficient is investigated in the limit that Reynolds number approaches infinity. The simulation results suggest that the ideal slip length coefficient may be plateauing to a finite value in the infinite Reynolds number limit.

**Acknowledgments**

This work is supported by NASA Transformational Tools and Technologies grant #80NSSC20M0201.

REFERENCES

Bae, H. J., Lozano-Durán, A., Bose, S. T. & Moin, P. 2019 Dynamic slip wall model for large-eddy simulation. *J. Fluid Mech.* **859**, 400–432.

Bose, S. T. & Moin, P. 2014 A dynamic slip boundary condition for wall-modeled large-eddy simulation. *Phys. Fluids* **26**, 015104.

Bose, S. T. & Park, G. I. 2018 Wall-modeled large-eddy simulation for complex turbulent flows. *Annu. Rev. Fluid Mech.* **50**, 535–561.

Cabot, W. H. & Moin, P. 2000 Approximate wall boundary conditions in the large-eddy simulation of high Reynolds number flow. *Flow Turbul. Combust.* **63**, 269–291.

del Álamo, J. C. & Jiménez, J. 2003 Spectra of the very large anisotropic scales in turbulent channels. *Phys. Fluids* **15**, L41–L44.

Germano, M. 1986 Differential filters for the large eddy numerical simulation of turbulent flows. *Phys. Fluids* **29**, 1755–1757.

Germano, M., Piomelli, U., Moin, P. & Cabot, W. H. 1991 A dynamic subgrid-scale eddy viscosity model. *Phys. Fluids A* **3**, 1760–1765.

Hoyas, S. & Jiménez, J. 2006 Scaling of the velocity fluctuations in turbulent channels up to $Re_\tau = 2000$. *Phys. Fluids* **18**, 011702.

Hoyas, S. & Jiménez, J. 2008 Reynolds number effects on the Reynolds-stress budgets in turbulent channels. *Phys. Fluids* **20**, 101511.

Hoyas, S., Oberlack, M., Kraheberger, S., Alcantara-Avila, F. & Laux, J. 2022 Wall turbulence at high friction Reynolds numbers. *Phys. Rev. Fluids* **7**, 014602.

Lee, M. & Moser, R. D. 2015 Direct numerical simulation of turbulent channel flow up to $Re_\tau = 5200$. *J. Fluid Mech.* **774**, 395–415.

Lozano-Durán, A. & Jiménez, J. 2014 Effect of the computational domain on direct simulations of turbulent channels up to $Re_\tau = 4200$. *Phys. Fluids* **26**, 011702.

Marusic, I. & Monty, J. P. 2019 Attached eddy model of wall turbulence. *Annu. Rev. Fluid Mech.* **51**, 49–74.

Monkewitz, P. A. 2017 Revisiting the quest for a universal log-law and the role of pressure gradient in "canonical" wall-bounded turbulent flows. *Phys. Rev. Fluids* **2**, 094602.

Moser, R. D., Kim, J. & Mansour, N. N. 1999 Direct numerical simulation of turbulent channel flow up to $Re_\tau = 590$. *Phys. Fluids* **11**, 943–945.

Oberlack, M., Hoyas, S., Kraheberger, S., Alcantara-Avila, F. & Laux, J. 2022 Turbulence statistics of arbitrary moments of wall-bounded shear flows: a symmetry approach. *Phys. Rev. Lett.* **128**, 024502.

Pradhan, A. & Duraisamy, K. 2022 A unified understanding of scale-resolving simulations and near-wall modelling of turbulent flows using optimal finite-element projections. *J. Fluid Mech.* **955**, A6.

Pullin, D. I., Inoue, M. & Saito, N. 2013 On the asymptotic state of high Reynolds number, smooth-wall turbulent flows. *Phys. Fluids* **25**, 015116.

Uzun, A. & Malik, M. 2022 High-fidelity simulation of turbulent flow past Gaussian bump. *AIAA J.* **60**, 2130–2149.

Vreman, A. W. 2004 An eddy-viscosity subgrid-scale model for turbulent shear flow: algebraic theory and applications. *Phys. Fluids* **16**, 3670–3681.

White, F. M. 2011 *Viscous Fluid Flow*, 3rd Ed. McGraw-Hill Education.

Whitmore, M. P., Bose, S. T. & Moin, P. 2022 Progress on slip wall modeled LES for predicting smooth body separation. *Annual Research Briefs*, Center for Turbulence Research, Stanford University, pp. 59–70.

Whitmore, M. P., Griffin, K. P., Bose, S. T. & Moin, P. 2021 Large-eddy simulation of a Gaussian bump with slip-wall boundary conditions. *Annual Research Briefs*, Center for Turbulence Research, Stanford University, pp. 45–58.

Yang, X. I. A., Bose, S. & Moin, P. 2016 A physical basis of the slip-wall model for wall-modeled large-eddy simulations. *Annual Research Briefs*, Center for Turbulence Research, Stanford University, pp. 65–74.